Advances in Water Resources 178 (2023) 104491

Contents lists available at ScienceDirect

Advances in Water Resources

journal homepage: www.elsevier.com/locate/advwatres

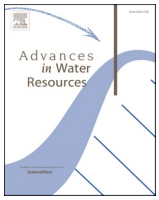

Watertable fluctuations in coastal unconfined aquifers with a sloping sea boundary: Vertical flow and dynamic effective porosity effects

Zhaoyang Luo [a,b,d,*], Jun Kong [c], D.A. Barry [d,*]

[a] College of Science and Engineering, Flinders University, Adelaide, Australia
[b] National Centre for Groundwater Research and Training, Adelaide, Australia
[c] Key Laboratory of Coastal Disaster and Protection (Ministry of Education), Hohai University, Nanjing, China
[d] Faculty of Architecture, Civil and Environmental Engineering (ENAC), Ecological Engineering Laboratory (ECOL), Environmental Engineering Institute (IIE), École Polytechnique Fédérale de Lausanne (EPFL), Lausanne, Switzerland

ARTICLE INFO

Keywords:
Analytical solution
Numerical simulation
Amplitude decay
Phase lag
Overheight

ABSTRACT

Interactions between the tide and sloping sea boundary make watertable fluctuations in coastal unconfined aquifers complicated. Based on a perturbation method, we derived a new analytical solution to predict watertable fluctuations for coastal unconfined aquifers with a sloping sea boundary. Following validation with a numerical model, the analytical solution was used to explore the effects of the vertical flow (in the saturated zone) and dynamic effective porosity on watertable fluctuations. Results show that the new analytical solution accurately predicts watertable fluctuations for coastal unconfined aquifers with a sloping sea boundary. Compared with sand coastal unconfined aquifers, both vertical flow and dynamic effective porosity effects on watertable fluctuations are more pronounced for loam coastal unconfined aquifers. Vertical flow has a minor influence on the fluctuation amplitude while it significantly decreases the phase lag of the watertable fluctuation at a given location. In contrast to vertical flow, accounting for the dynamic effective porosity not only decreases the phase lag, but also significantly amplifies the fluctuation amplitude for a given location, which enables watertable wave propagation further inland. Increasing the beach slope weakens the effects of the vertical flow and dynamic effective porosity on watertable fluctuations. Furthermore, including either the vertical flow or dynamic effective porosity effects leads to a lower watertable overheight. These results highlight the importance of vertical flow and dynamic effective porosity effects in models of watertable fluctuations.

1. Introduction

Coastal unconfined aquifers are hotspots for land-ocean interactions. Subject to oceanic oscillations (e.g., tides and waves), water periodically flows into or drains out of coastal unconfined aquifers, leading to watertable fluctuations that directly impact a range of groundwater-dependent processes such as beach erosion, seawater intrusion, submarine groundwater discharge, solute transport and chemical loading to the ocean (e.g., Parlange et al. 1984, Li et al. 1999, Moore 2010, Xin et al. 2010, Bakhtyar et al. 2011, Werner et al. 2013, Robinson et al. 2018). An accurate prediction of watertable fluctuations is essential for understanding these groundwater-dependent processes.

Previously, substantial efforts were devoted to predicting watertable fluctuations in coastal unconfined aquifers (e.g., Parlange et al. 1984, Nielsen 1990, Barry et al., 1996, Raubenheimer et al. 1999, Li et al. 2000a, b, Robinson et al. 2006, Heiss and Michael 2014, Shoushtari et al. 2016, Luo et al. 2023). Most of these studies investigated watertable fluctuations based on the one-dimensional Boussinesq equation since it is computationally efficient and reveals explicit relations between parameters that affect watertable fluctuations. Initially, the Boussinesq equation was used to describe groundwater flow in the saturated zone (e.g., Parlange et al. 1984, Nielsen 1990, Bear 2012). With time, more laboratory and field data were presented, and it was found that the predictions of the classical Boussinesq equation deviate from measurements. Therefore, the Boussinesq equation was extended to account for different factors including the vertical flow (in the saturated zone) (e.g., Nielsen et al. 1997, Li et al. 2000b), unsaturated flow (e.g., Parlange and Brutsaert 1987, Barry et al., 1996, Li et al. 1997,

* Corresponding authors at: Faculty of Architecture, Civil and Environmental Engineering (ENAC), Ecological Engineering Laboratory (ECOL), Environmental Engineering Institute (IIE), École Polytechnique Fédérale de Lausanne (EPFL), Lausanne, Switzerland.
E-mail addresses: zhaoyang.luo666@gmail.com (Z. Luo), andrew.barry@epfl.ch (D.A. Barry).

https://doi.org/10.1016/j.advwatres.2023.104491
Received 5 March 2023; Received in revised form 12 June 2023; Accepted 14 June 2023
Available online 15 June 2023

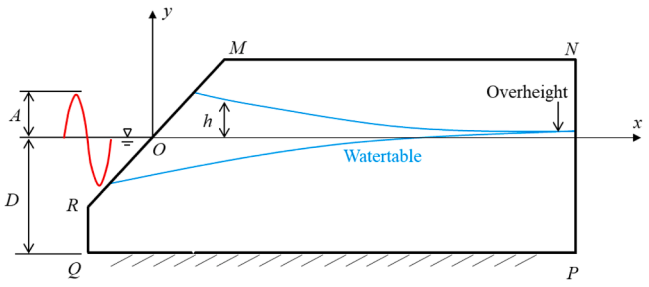

Fig. 1. Conceptual model of coastal unconfined aquifers with a sloping sea boundary (*MRQ*). *MN* is the atmospheric boundary, and both *QP* and *PN* are no-flow boundaries.

Table 1
Definitions of M_j, N_j, V_j, W_j and P_j.

j	M_j	N_j	V_j	W_j	P_j
1	$-Ak_1\sqrt{\frac{K_sD\omega}{2n_t}}$	$-Ak_2\sqrt{\frac{K_sD\omega}{2n_t}}$	$-k_1$	2ω	$-k_2$
2	$Ak_1\sqrt{\frac{K_sD\omega}{2n_t}}$	$Ak_2\sqrt{\frac{K_sD\omega}{2n_t}}$	$-k_1$	0	$-k_2$

Table 2
Soil Parameters.

Soils	n_e	K_s (m s^{-1})	α (m^{-1})	n	α_1 (m^{-1})	n_1	H_ψ (m)
Laboratory sand[a]	0.3	1.32×10^{-4}	1.7	9	1.63	8.27	0.61
Sand	0.4	3×10^{-3}	11	6	10	5.23	0.1
Loam	0.23	4.27×10^{-5}	4.37	2.22	1.58	1.34	0.66

[a] Sand used in the experiment of Cartwright et al. (2004).

Jeng et al. 2005b, Kong et al. 2013, 2015) and hysteresis (e.g., Kong et al. 2016a). Watertable fluctuations in coastal unconfined aquifers predicted using Boussinesq-based equations show an asymptotic amplitude decay rate and zero phase lag increase rate (standing wave behavior) of watertable waves with increasing $n_e\omega D/K_s$ (where n_e [-] is the static effective porosity, $\omega = 2\pi/T$ [T^{-1}] is the angular frequency with T [T] being the fluctuation period, D [L] is the mean sea level height and K_s [LT^{-1}] is the saturated hydraulic conductivity) (e.g., Barry et al., 1996, Nielsen et al. 1997, Li et al. 2000a, Kong et al. 2013, 2015). However, this limiting behavior was not found in the laboratory experiments of Shoushtari et al. (2016), in which fluctuation period effects (i.e., $n_e\omega D/K_s$) on watertable wave propagation in the unconfined aquifer with a vertical sea boundary were considered. Shoushtari et al. (2016) observed an increase of both the amplitude decay rate and phase lag increase rate of watertable waves with increasing $n_e\omega D/K_s$ and hence concluded that all existing Boussinesq equations cannot predict experimental results correctly.

Effective porosity is the volume of water that an aquifer drains or imbibes per unit surface area of aquifer per unit change of the watertable height (Childs, 1960). It is usually treated as a constant (e.g., Barry et al., 1996, Nielsen et al. 1997, Li et al., 2000a, Kong et al. 2013, 2015). Nevertheless, experimental, field and numerical evidence show that the effective porosity depends on the porewater velocity during watertable fluctuations (e.g., Cartwright et al. 2005, Rabinovich et al. 2015, Pozdniakov et al. 2019). More recently, Luo et al. (2023) developed a modified Boussinesq equation that includes vertical flow and dynamic effective porosity effects, and showed that its predictions compare well with a wide range of experimental data compiled from Parlange et al. (1984), Cartwright et al. (2003), Shoushtari et al. (2016) and Kong et al. (2016a), i.e., the modified Boussinesq equation accurately predicts

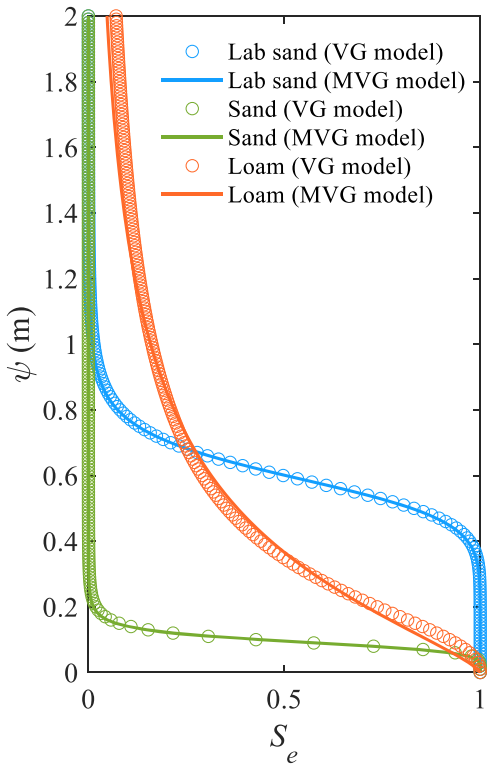

Fig. 2. Comparison between the VG and MVG models for different soils listed in Table 2.

watertable fluctuations for coastal unconfined aquifers with a vertical sea boundary, including for large $n_e\omega D/K_s$.

Most of abovementioned work regarding watertable fluctuations assumes a vertical sea boundary, although sloping beaches are common (Vos et al., 2020). Nielsen (1990) developed an analytical approximation to predict watertable fluctuations in coastal unconfined aquifers with a sloping sea boundary using a perturbation method. However, this analytical solution only matches the time-varying sea boundary condition approximately. To overcome this shortcoming, Li et al. (2000a) revisited the same linearized Boussinesq equation and derived an analytical solution using a coordinate transformation that enables inclusion of moving boundary effects. Kong et al. (2011) obtained an analytical solution based on a nonlinear Boussinesq equation by a perturbation method with two perturbation parameters, alleviating high-order term problems in the analytical solutions of Nielsen (1990) and Li et al. (2000a). In addition to solutions based on the Boussinesq equation, Teo et al. (2003) and Jeng et al. (2005a, b) derived analytical solutions based on Laplace's equation for coastal unconfined aquifers with a sloping sea boundary. They did not, however, consider the vertical flow and dynamic effective porosity that, for a vertical sea boundary, affect watertable fluctuations (Luo et al., 2023), as mentioned above.

Here, based on a modified Boussinesq equation that includes vertical flow and dynamic effective porosity effects (Luo et al., 2023), an analytical solution is derived for coastal unconfined aquifers with a sloping sea boundary by a perturbation method. After comparison with a well-validated numerical model, the new analytical solution is used to explore the effects of vertical flow and dynamic effective porosity on watertable fluctuations for coastal unconfined aquifers with a sloping sea boundary.

Table 3
Parameters adopted in numerical simulations.

Case	Base	1	2	3	4
Beach slope (°)	11.7	11.7	11.7	11.7	11.7
A (m)	0.204	0.204	0.204	0.204	0.204
T (s)	348	1800	7200	21,600	43,200
Aquifer length (m)	9	50	50	50	50
Aquifer height (m)	1.5	1.5	1.5	1.5	1.5
D (m)	1.01	1.01	1.01	1.01	1.01
Mesh size (m)	0.02, 0.0071–0.015[a]	0–9 m: the same as the base case 9–50 m: 0.2, 0.015	0–9 m: the same as the base case 9–50 m: 0.2, 0.015	0–9 m: the same as the base case 9–50 m: 0.2, 0.015	0–9 m: the same as the base case 9–50 m: 0.2, 0.015
Time step (s)	4	4	8	15	30
Soil[b]	Laboratory sand	Laboratory sand	Laboratory sand	Laboratory sand	Laboratory sand
Residual water saturation	0.05	0.05	0.05	0.05	0.05

[a] Vertical distance of the mesh varies from the sea to the inland.
[b] Soil parameters listed in Table 2.

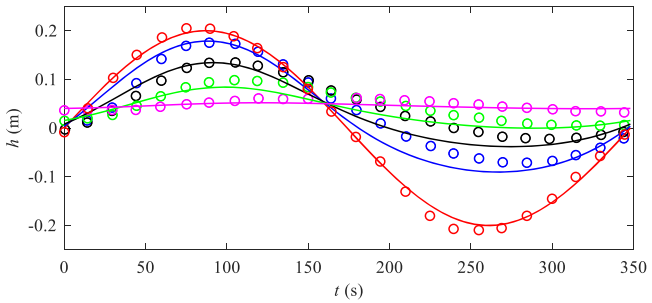

Fig. 3. Comparison of simulated (lines, SUTRA) and measured watertable (circles, Cartwright et al., 2004) at $x = 0$ m (red), 0.4 m (blue), 1.4 m (black), 2.4 m (green) and 3.4 m (pink). All locations are 0.1 m from the bottom boundary in the vertical direction.

2. Theory

2.1. Governing equation

To account for the vertical flow and dynamic effective porosity effects, watertable fluctuations in homogeneous coastal unconfined aquifers with a sloping sea boundary (Fig. 1) can be described by a modified Boussinesq equation (Luo et al., 2023),

$$n_t \frac{\partial h}{\partial t} = K_s D \frac{\partial^2 h}{\partial x^2} + K_s D^3 \frac{\partial^4 h}{\partial x^4} \tag{1a}$$

with

$$n_t = n_e \left[1 - \exp\left[- \left(\frac{a}{\tau_\omega} \right)^b \right] \right] \tag{1b}$$

$$\tau_\omega = \frac{n_e H_\psi / K_s}{1/\omega} = \frac{n_e \omega H_\psi}{K_s} \tag{1c}$$

$$H_\psi = \int_0^\infty \frac{\theta - \theta_r}{\theta_s - \theta_r} d\psi \tag{1d}$$

where h [L] is the watertable elevation relative to the mean sea level, t [T] is time, x [L] is the horizontal distance from the origin, n_t [-] is the dynamic effective porosity, τ_ω [-] is a dimensionless parameter related to the watertable fluctuation frequency and soil properties, a [-] and b [-] are fitting parameters, H_ψ [L] is a measure of the equivalent saturated height of the unsaturated zone, θ [-] is the soil water content related to the capillary suction ψ [L], and θ_s and θ_r are the saturated and residual soil water contents, respectively. Note that the fourth-order term in the right-hand side and n_t in Eq. (1a) represent vertical flow and dynamic effective porosity effects, respectively.

Various models have been proposed to describe the relation between θ and ψ. Among these, van Genuchten (1980)'s model (VG model) is widely used and can be written as,

$$\theta = (\theta_s - \theta_r) S_e + \theta_r = (\theta_s - \theta_r)[1 + (\alpha\psi)^n]^{-1+1/n} + \theta_r \tag{2}$$

where α [L^{-1}] and n [-] are the fitting parameters related to soil properties, and S_e [-] is the effective saturation. However, substituting Eq. (2) into Eq. (1d) does not lead to simple analytical expression, but requires numerical treatment. Therefore, a modified van Genuchten model (MVG model) is adopted to describe the relation between θ and ψ (Troch, 1993; Kong et al., 2016b; Luo et al., 2019),

$$\theta = (\theta_s - \theta_r) S_e + \theta_r = (\theta_s - \theta_r)[1 + (\alpha_1\psi)^{n_1}]^{-1-1/n_1} + \theta_r \tag{3}$$

where α_1 [L^{-1}] and n_1 [-] are fitting parameters (different from α and n). The comparison between the VG and MVG model will be presented in the following section. By comparison, the difference between the MVG model and VG model is the exponent, which makes the MVG model integrable to attain simple analytical expression, i.e., substituting Eq. (3) into Eq. (1d) gives (Luo et al., 2019),

$$H_\psi = \frac{1}{\alpha_1} \tag{4}$$

2.2. Analytical derivation

In contrast to aquifers with a vertical sea boundary, sea level oscillations on a sloping beach generate a moving boundary condition,

$$h[\cot(\beta)\eta(t), t] = \eta(t) \tag{5}$$

where η [m] is the sea level relative to the mean sea level and β [-] is the beach slope. Following Li et al. (2000a), the moving boundary is considered by transforming the coordinate as,

$$z = x - \cot(\beta)\eta(t) \tag{6}$$

For simplicity, a driving head modeled as a cosine function is assumed at the sea boundary,

$$h(0, t) = \eta(t) = A\cos(\omega t) \tag{7}$$

where A [L] is the amplitude of the driving head. Combining Eqs. (6) and (7) and substituting into Eq. (1a) gives,

$$\frac{\partial h}{\partial t} = \frac{K_s D}{n_t} \frac{\partial^2 h}{\partial z^2} + \frac{K_s D^3}{3 n_t} \frac{\partial^4 h}{\partial z^4} - A\omega\cot(\beta)\sin(\omega t) \frac{\partial h}{\partial z} \tag{8}$$

The perturbation parameter used in approximating the solution to Eq. (8) subject to Eq. (7) is:

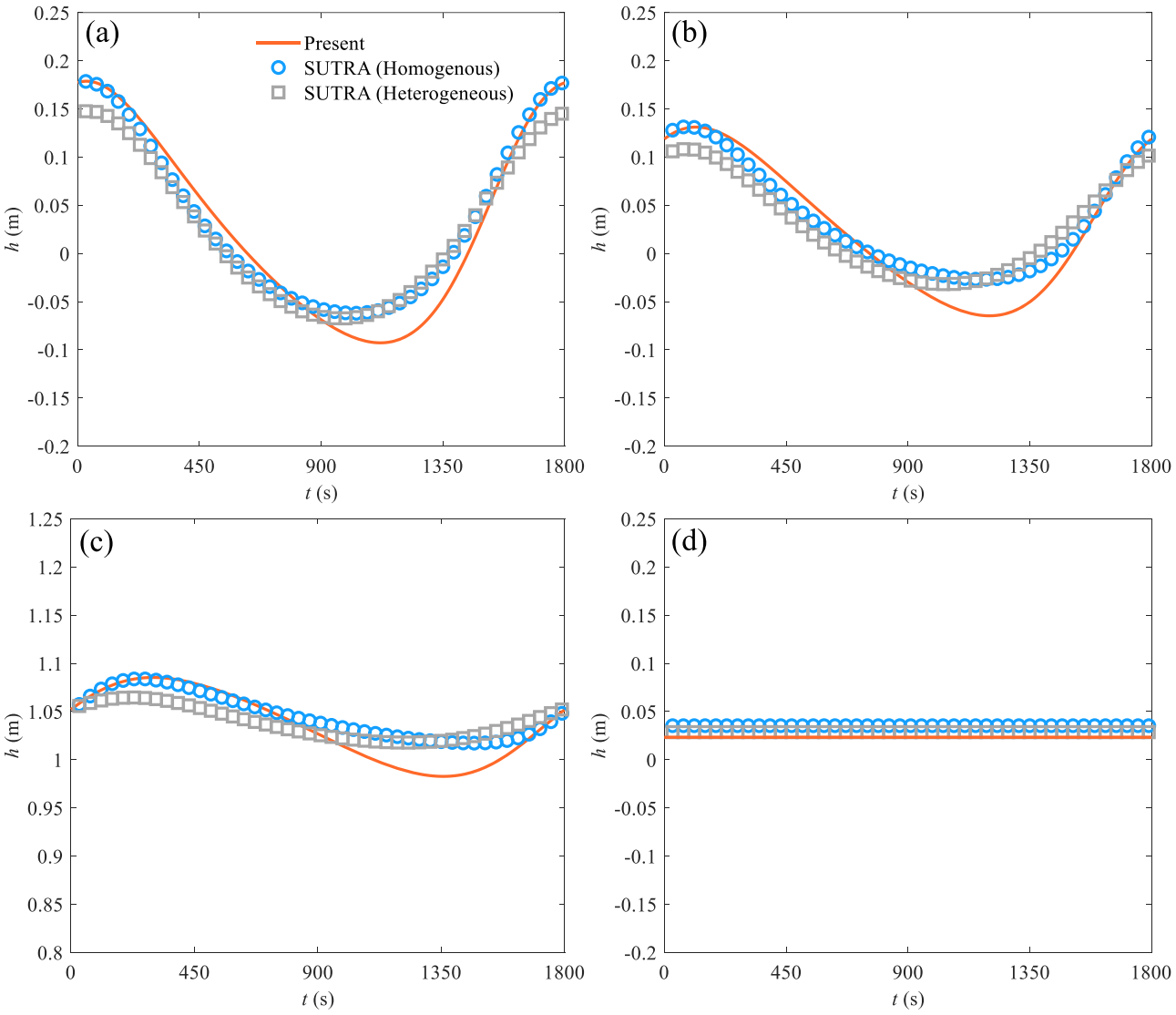

Fig. 4. Watertable predicted by SUTRA with homogenous and heterogeneous soils and the present analytical solution at x = (a) 1.4 m, (b) 2.4 m, (c) 4.4 m and (d) 47.55 m for T = 1800s.

$$\varepsilon = A\sqrt{\frac{n_t\omega}{2K_sD}}\cot(\beta) \tag{9}$$

Compared with the perturbation parameter adopted in previous studies (Nielsen, 1990; Li et al., 2000a), n_t, rather than n_e is involved in Eq. (9). Therefore, the modified ε is less than or equal to the original one because of a smaller n_t. Note that ε is required to be less than unity when using the perturbation approach. Physically, ε is the ratio of tidal excursion to the wavelength of primary wave (Li et al., 2000a).

Combining Eqs. (8) and (9) gives,

$$\frac{\partial h}{\partial t} = \frac{K_sD}{n_t}\frac{\partial^2 h}{\partial z^2} + \frac{K_sD^3}{3n_t}\frac{\partial^4 h}{\partial z^4} - \sqrt{\frac{2K_s\omega D}{n_t}}\varepsilon\sin(\omega t)\frac{\partial h}{\partial z} \tag{10}$$

Consistent with Li et al. (2000a), we seek a solution of the form,

$$h = h_0 + \varepsilon h_1 + O(\varepsilon^2) \tag{11}$$

where h_0 and h_1 are the zeroth and first-order solutions, respectively.

2.3. Zeroth-order solution

By substituting Eq. (10) into Eq. (11), the following zeroth-order perturbation equation is obtained,

$$\frac{\partial h_0}{\partial t} = \frac{K_sD}{n_t}\frac{\partial^2 h_0}{\partial z^2} + \frac{K_sD^3}{3n_t}\frac{\partial^4 h_0}{\partial z^4} \tag{12}$$

The corresponding boundary condition is,

$$h_0(0,t) = A\cos(\omega t) \tag{13}$$

The solution of Eq. (12) subject to Eq. (13) is (Nielsen et al., 1997; Luo et al., 2023),

$$h_0 = A\exp(-k_1z)\cos(\omega t - k_2z) \tag{14a}$$

with

$$kD = (k_1 + k_2i)D = \sqrt{\frac{3}{2}}\sqrt{-1 + \sqrt{1 + \frac{4}{3}\frac{n_t\omega D}{K_s}i}} \tag{14b}$$

where $k = k_1 + ik_2$ is the watertable wave number with $i = \sqrt{-1}$. The real (k_1D) and imaginary (k_2D) parts represent the amplitude decay rate and phase lag increase rate of the zeroth-order wave, respectively.

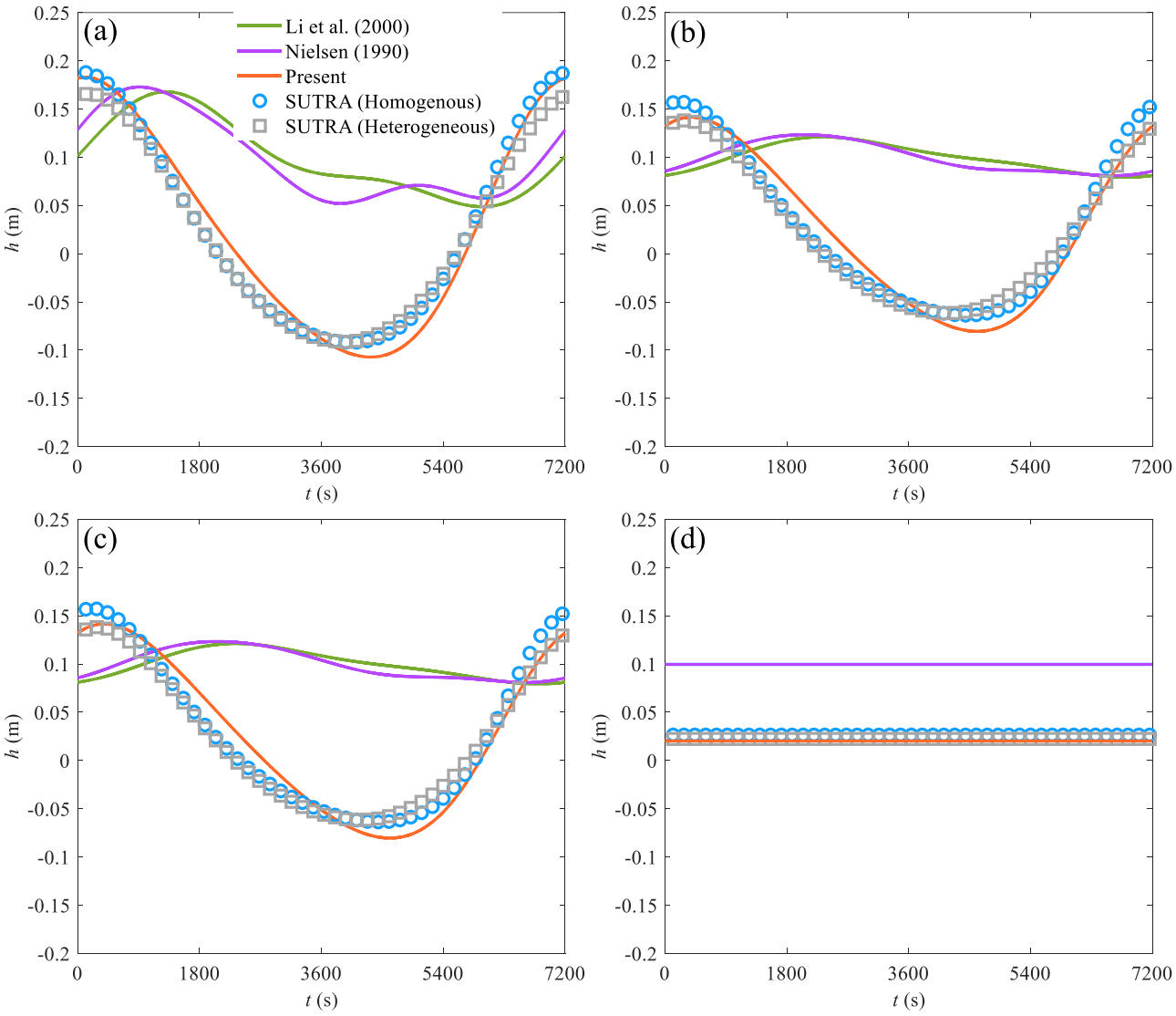

Fig. 5. Watertable predicted by SUTRA with homogenous and heterogeneous soils and various analytical solutions at x = (a) 1.4 m, (b) 2.4 m, (c) 4.4 m and (d) 47.55 m for $T = 7200$ s.

2.4. First-order solution

Similarly, substituting Eq. (10) into Eq. (11) gives the following first-order perturbation equation,

$$\frac{\partial h_1}{\partial t} = \frac{K_s D}{n_t}\frac{\partial^2 h_1}{\partial z^2} + \frac{K_s D^3}{3n_t}\frac{\partial^4 h_1}{\partial z^4} - \sqrt{\frac{2K_s\omega D}{n_t}}\sin(\omega t)\frac{\partial h_0}{\partial z} \tag{15}$$

The corresponding boundary condition is,

$$h_1(0,t) = 0 \tag{16}$$

Since the amplitude of the first-order wave is much less than that of the zeroth-order wave, the second term on the right-hand side of Eq. (15) can be ignored and hence Eq. (15) is approximated as,

$$\frac{\partial h_1}{\partial t} = \frac{K_s D}{n_t}\frac{\partial^2 h_1}{\partial z^2} - \sqrt{\frac{2K_s\omega D}{n_t}}\sin(\omega t)\frac{\partial h_0}{\partial z} \tag{17}$$

Substituting Eq. (14a) into Eq. (17) yields,

$$\frac{\partial h_1}{\partial t} = \frac{K_s D}{n_t}\frac{\partial^2 h_1}{\partial z^2} - \sum_{j=1}^{2}\left[M_j \exp(V_j z)\sin(W_j t + P_j z) + N_j \exp(V_j z)\cos(W_j t + P_j z)\right] \tag{18}$$

where $j = 1$ or 2 and expressions for M_j, N_j, V_j, W_j and P_j are given in Table 1.

Since Eq. (18) is linear, h_1 can be divided into,

$$h_1 = h_{11} + h_{12} \tag{19}$$

The solution to h_{1j} ($j = 1$ or 2) is,

$$h_{1j} = \mathrm{Y}\exp(V_j z)\cos(W_j t + P_j z) - \mathrm{Y}\exp(Fz)\cos(W_j t + Fz) + \Gamma\exp(V_j z)\sin(W_j t + P_j z) - \Gamma\exp(Fz)\sin(W_j t + Fz) \tag{20a}$$

with

$$E = \frac{K_s D}{n_t} \tag{20b}$$

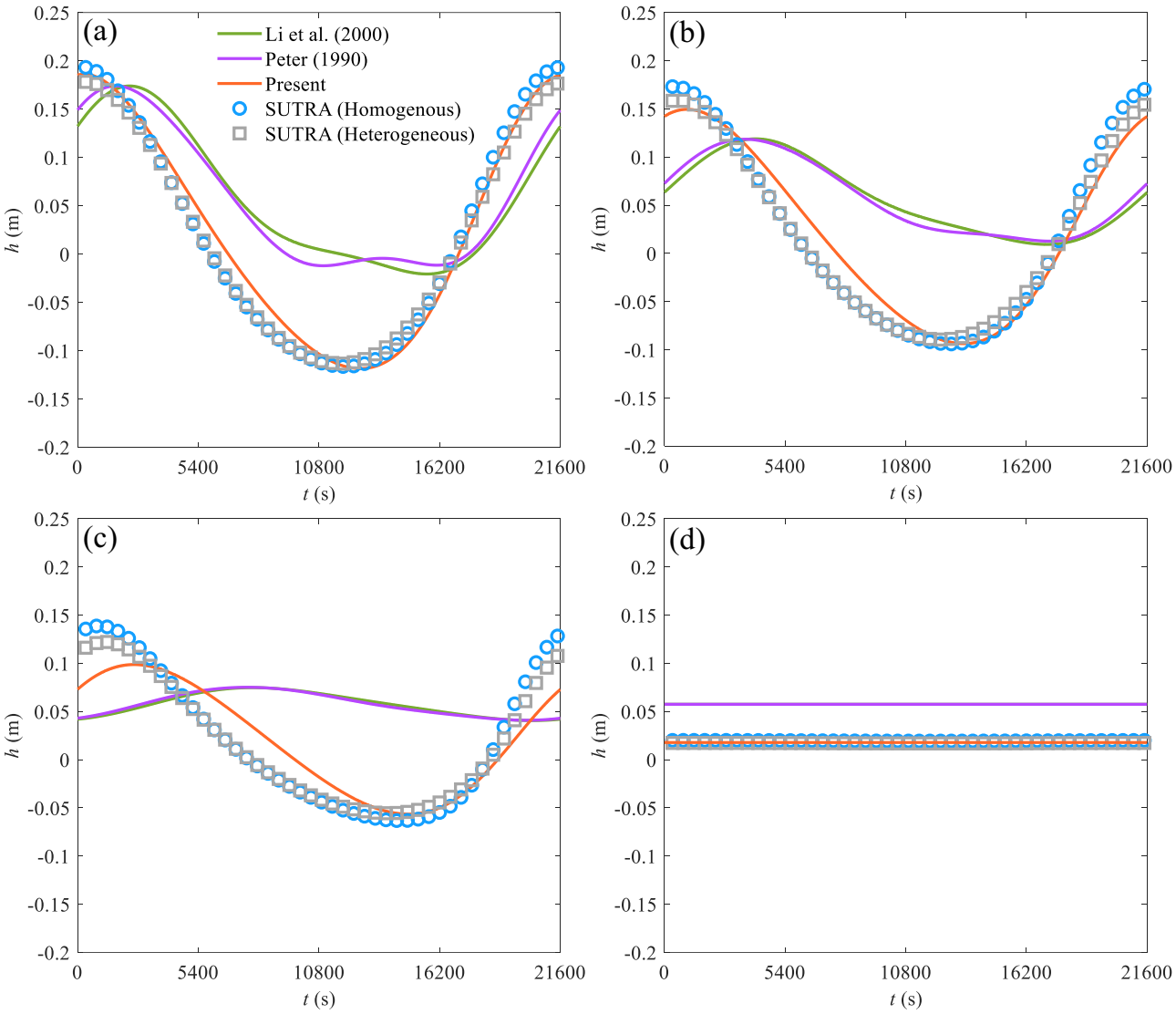

Fig. 6. Watertable predicted by SUTRA with homogenous and heterogeneous soils and various analytical solutions at x = (a) 1.4 m, (b) 2.4 m, (c) 4.4 m and (d) 47.55 m for T = 21,600 s.

$$\Upsilon = \frac{\left(V_j^2E - P_j^2E\right)N_j - \left(2P_jV_jE - W_j\right)M_j}{\left(V_j^2E - P_j^2E\right)^2 + \left(2P_jV_jE - W_j\right)^2} \tag{20c}$$

$$\Gamma = \frac{\left(2P_jV_jE - W_j\right)N_j + \left(V_j^2E - P_j^2E\right)M_j}{\left(V_j^2E - P_j^2E\right)^2 + \left(2P_jV_jE - W_j\right)^2} \tag{20d}$$

$$F = -\sqrt{\frac{W_j}{2E}} \tag{20e}$$

Substituting Eqs. (14), (19) and (20) into Eq. (11) gives the analytical expression of h. Note that Eqs. (14a) and (20a) include the independent variable, z. To obtain the analytical solution in the original x-coordinate, one only needs to substitute Eq. (6) into Eqs. (14a) and (20a), respectively.

3. Analytical validation

In contrast to various existing laboratory experiments concerning watertable fluctuations in coastal unconfined aquifers with a vertical beach (e.g., Parlange et al. 1984, Cartwright et al. 2003, Kong et al. 2016b, Shoushtari et al. 2016), experimental measurements with a sloping beach are scarce. Therefore, we first validate the numerical model by a laboratory experiment and then compare the analytical solution with the validated numerical model.

3.1. Comparison between measurements and numerical simulations

Cartwright et al. (2004) conducted laboratory experiments of watertable wave propagation in the coastal unconfined aquifer with a sloping beach of 11.7°. In their experiment, the sand flume had dimensions of 9 m (length) × 0.12 m (width) × 1.5 m (height). The mean sea level was set to 1.01 m from the aquifer bottom. A driving head with an amplitude of 0.204 m and a period of 348 s was imposed on the sea boundary, creating a moving boundary because of the sloping beach. The sand used in the experiment had an average saturated hydraulic conductivity of 1.32×10^{-4} m s^{-1} and a static effective porosity of 0.3. The VG model fitting parameters were 1.7 m^{-1} and 9. Fitting the MVG model to the VG model gives $\alpha_1 = 1.63$ m^{-1} and $n_1 = 8.2$ with which the MVG model matches well with the VG model (Table 2 and Fig. 2). The saturated and residual soil water contents were 0.38 and 0.08, respectively. Based on the experimental setup, ε was 4.44 without considering the dynamic effective porosity. A smaller ε results for the dynamic

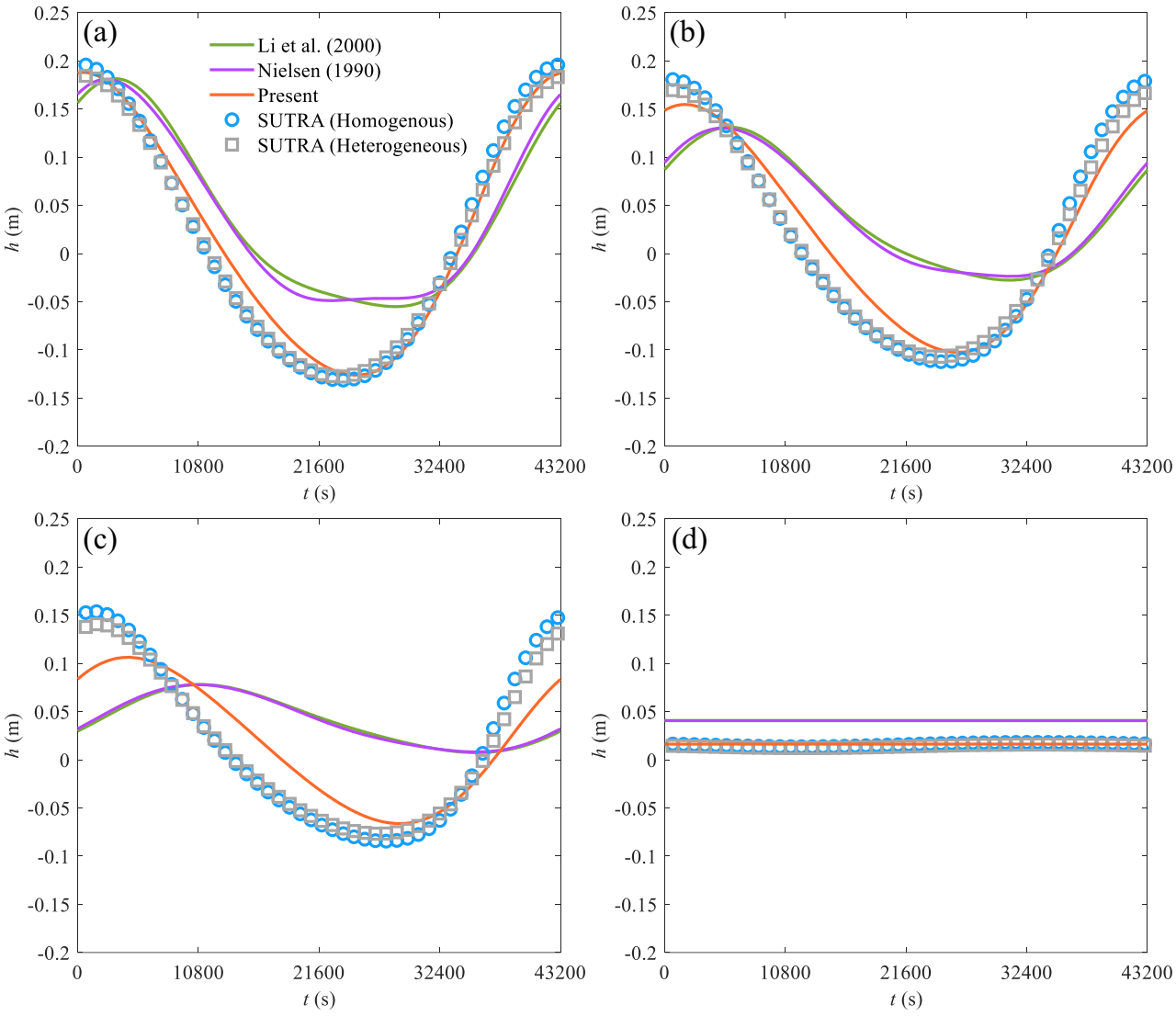

Fig. 7. Watertable predicted by SUTRA with homogenous and heterogeneous soils and various analytical solutions at x = (a) 1.4 m, (b) 2.4 m, (c) 4.4 m and (d) 47.55 m for T = 43,200 s.

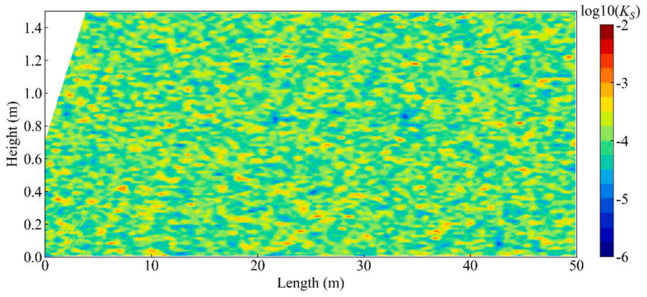

Fig. 8. A log-normal hydraulic conductivity field with a mean value of 1.32 × 10^{-4} m/s, a variance of 1 and a horizontal correction length of 5 m.

effective porosity, but it was still close to unity with the a and b values determined in the next section. Thus, the new analytical solution cannot be used to predict the experiment of Cartwright et al. (2004) directly.

A 3-D variable-saturation and variable-density groundwater model, SUTRA (Voss and Provost, 2010), was used to simulate the experiment of Cartwright et al. (2004) using the setup in Fig. 1. In the numerical simulations, *MRQ* was treated as a time-varying boundary condition. *MN* was the atmospheric boundary while *QP* and *PN* were no-flow boundaries. Initially, the pressure distribution was hydrostatic relative to the sea level. The seepage face on *MRQ* was implemented into the numerical model following the method of Xin et al. (2010). The model domain was discretized with a horizontal distance of 0.02 m (450 columns) and vertical distance varying from 0.0071 to 0.015 m (100 layers) (Case Base in Table 3). The numerical simulation was run to get quasi-steady state with a time step of 4 s. Different mesh sizes and time steps were tested to ensure grid-independent numerical results.

Fig. 3 compares simulated and measured watertables at different locations. In general, the numerical predictions are in good agreement with the measurements of Cartwright et al. (2004), especially during the watertable raising stage. However, there are deviations between predicted and measured results during the falling watertable stage, suggesting the numerical model cannot capture the seepage face accurately. This is likely because truncation of the unsaturated zone in the sloping beach area may have introduced errors in predicting the watertable dynamics based on the original Richards' equation (Zheng et al., 2022). Overall, the comparison between the numerical model and experiment enhances the confidence to adopt numerical results of SUTRA as benchmarks.

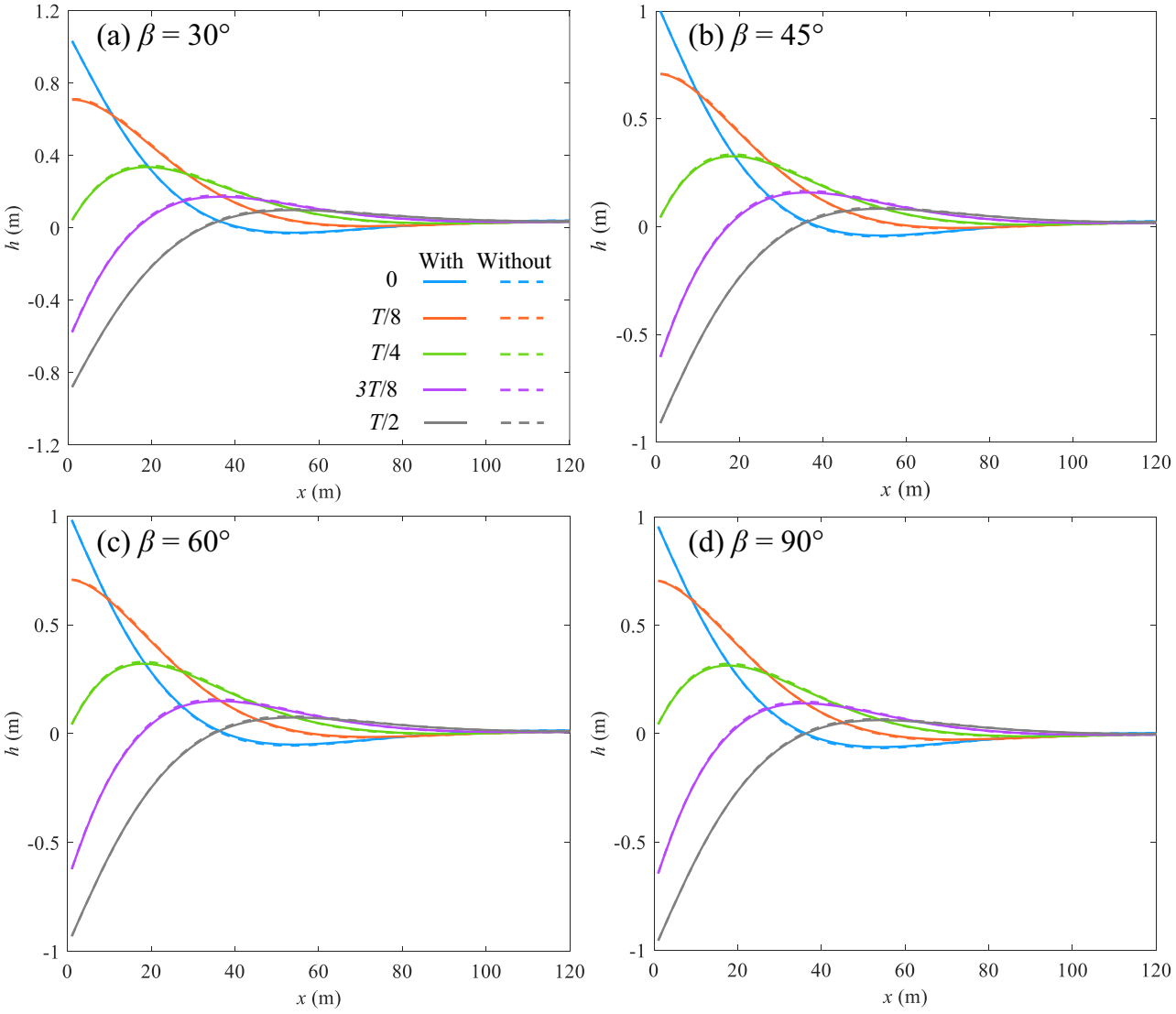

Fig. 9. Predicted watertable elevation distributions of sand coastal unconfined aquifers based on the analytical solutions with (solid lines) and without (Li et al., 2000a; dashed lines) considering vertical flow at five typical time slots: 0 (blue), $T/8$ (orange), $T/4$ (green), $3T/8$ (purple) and $T/2$ (gray). Each plot corresponds to a different sloping sea boundary: (a) 30°, (b) 45°, (c) 60° and (d) 90°.

3.2. Comparison between numerical simulations and analytical solutions

After being validated by the experiment, we used the numerical model to evaluate the new analytical solution. Previous studies indicated that the fluctuation period plays an important role in affecting watertable wave propagation in coastal unconfined aquifers (e.g., Li et al. 2000a, Shoushtari et al. 2016, Luo et al. 2023). Therefore, based on the experimental setup of Cartwright et al. (2004), four different fluctuation periods were considered: 1800, 7200, 21,600 and 43,200 s. As the fluctuation period increases, the watertable wave propagates further inland. To decrease possible reflection effects from the inland boundary, the length of the sand flume was extended to 50 m which allows the amplitude of watertable wave at the inland boundary to be damped to within 1% of the amplitude of the driving head. Other parameters were the same as those in the experiment of Cartwright et al. (2004).

For all numerical simulations, the grid size was the same as the base case for the first 9 m from the sea, whereas it became 0.2 m (horizontal) × 0.015 m (vertical) for the rest of the model domain. The time step was 4, 8, 15 and 30 s when the fluctuation period was 1800, 7200, 21,600 and 43,200 s, respectively. All parameters adopted in numerical simulations are summarized in Table 3.

Before applying the new analytical solution to predict watertable fluctuations, the two fitting parameters a and b must be determined. Due to a lack of measured data relating n_t and ω, a and b were determined by fitting the present analytical solution to the numerical results for period $T = 1800$s. Fig. 4 shows watertable predicted by the numerical simulation and the present analytical solution with $a = 0.0335$ and $b = 0.7444$ for this case. The results of the present analytical solution are generally in good agreement with the numerical predictions at four locations. Nevertheless, there are deviations between the analytical and numerical predictions, especially during the watertable falling stage. One possibility for this mismatch is that Eq. (1d) is proposed based on one-dimensional sand column experiments for which the fluctuation amplitude is constant and only vertical flow occurs. This is contrary to the watertable wave propagation in coastal unconfined aquifers with both horizontal and vertical flows and amplitude decay along the inland. In addition, watertable wave propagation becomes more complicated because of the nonlinear interactions between the driving signal and sloping beach, i.e., truncation of the unsaturated zone and seepage face development. These nonlinear interactions are ignored when deriving the present analytical solution.

Subsequently, $a = 0.0335$ and $b = 0.7444$ were substituted into the

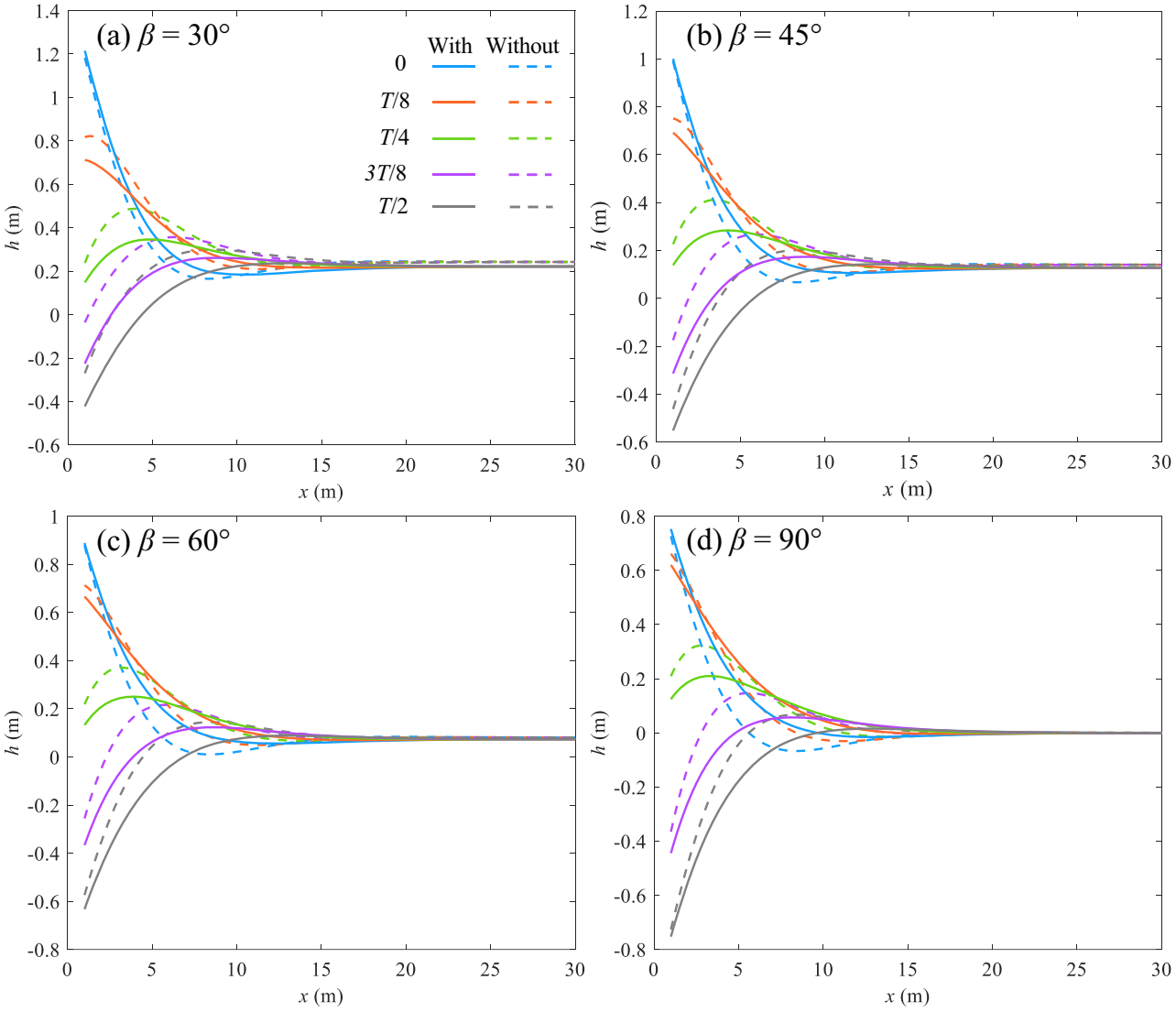

Fig. 10. Predicted watertable elevation distributions of loam coastal unconfined aquifers based on the analytical solutions with (solid lines) and without (Li et al., 2000a; dashed lines) considering the vertical flow at five typical time slots: 0 (blue), $T/8$ (orange), $T/4$ (green), $3T/8$ (purple) and $T/2$ (gray). Each plot corresponds to a different sloping sea boundary: (a) 30°, (b) 45°, (c) 60° and (d) 90°.

new analytical solution to predict watertable fluctuations with T = 7200, 21,600 and 43,200 s (Figs. 5–7). The results from the analytical solutions of Nielsen (1990) and Li et al. (2000a) are included for comparison. As can be seen, the new analytical solution performs well in reproducing the numerical results, while the Nielsen (1990) and Li et al. (2000a) analytical solutions significantly deviate from numerical predictions for all three cases (Figs. 5–7). This is because the analytical solutions of Nielsen (1990) and Li et al. (2000a) are derived from the original Boussinesq equation. When predicting watertable fluctuations from analytical solutions based on the original Boussinesq equation, the amplitude decay rate is equal to the phase lag increase rate for the zeroth-order fluctuation. This is contrary to the evidence from both field observations and laboratory experiments where the amplitude decay rate is different from the phase lag increase rate (Raubenheimer et al., 1999; Shoushtari et al., 2016; Luo et al., 2023). Moreover, neglecting the dynamic effective porosity leads to larger ε, which can increase errors of the analytical solution. Without the dynamic effective porosity, ε was calculated to be 0.9764, 0.5637 and 0.3986 for T = 7200, 21,600 and 43,200 s, respectively, whereas it decreased to 0.2026, 0.1777 and 01, 616 after considering the dynamic effective porosity. Note that predictions from the analytical solutions of Nielsen (1990) and Li et al. (2000a) are close to each other even though the latter captures moving boundary effects while the former does not.

Given that aquifers are usually heterogeneous, we further generated a log-normal hydraulic conductivity field with a mean value of 1.32×10^{-4} m/s (Fig. 8). Consistent with Yu et al. (2023), the variance and horizontal correction length of the log-normal hydraulic conductivity field were 1 and 5 m, respectively. Based on this log-normal hydraulic conductivity field, Cases 1–4 were re-simulated with other parameters kept the same. As can be seen from Figs. 4–7, the heterogeneity has minor influence on watertable for all cases. Consequently, the new analytical solution matches well with the numerical simulation even though the heterogeneity is considered.

The good performance of the new analytical solution confirms the applicability of Eqs. (1a) and (1d) even for the aquifer with a sloping sea boundary. Here, a = 0.0335 and b = 0.7444 were adopted to predict watertable fluctuations for the aquifer with a sloping beach of 11.7°. This differs from Luo et al. (2023) who found that Eq. (1a) with a = 0.0335 and b = 0.4444 can predict watertable wave propagation in coastal unconfined aquifers with a vertical sea boundary. This difference in the value of b occurs because the nonlinear interaction between the driving head and sloping beach affects watertable wave propagation and

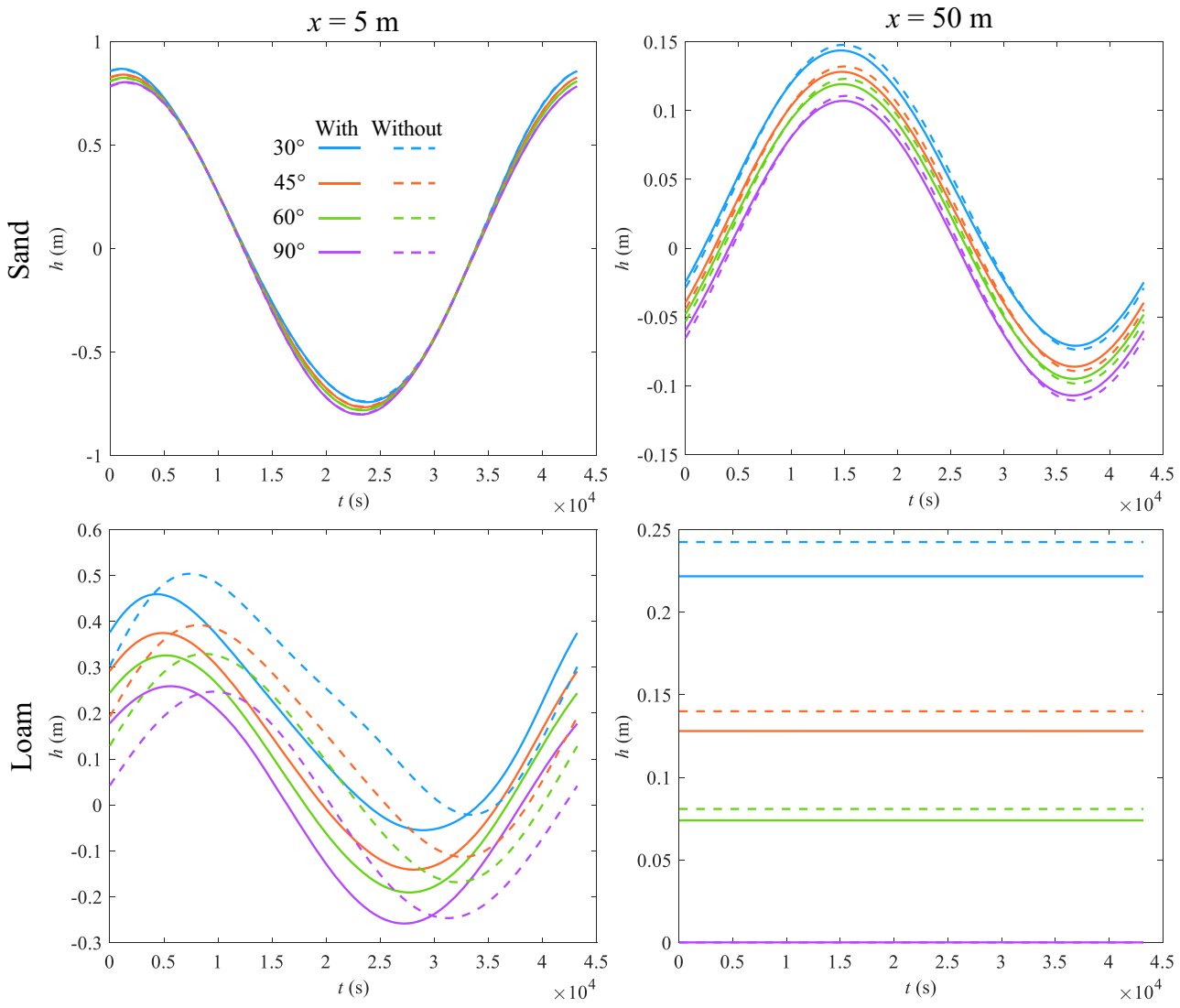

Fig. 11. Watertable elevation time series calculated from the analytical solutions with (solid lines) and without (Li et al., 2000a; dashed lines) considering vertical flow at $x = 5$ m (left panel) and 50 m (right panel) for sand (top panel) and loam (bottom panel) coastal unconfined aquifers with a different sloping sea boundary: 30° (blue), 45° (orange), 60° (green) and 90° (purple).

the water exchange between the saturated and unsaturated zones, thus leading to a different dynamic effective porosity. Despite this, with the groundwater level measured at a single location, a and b values can be readily determined by fitting the present analytical solution to watertable measurements. Therefore, the analytical solution presented here could be useful in real applications.

4. Hypothesized scenarios

Hypothesized scenarios were designed to illustrate the effects of the vertical flow and dynamic effective porosity on watertable fluctuations in coastal unconfined aquifers with a sloping sea boundary. In reality, tides usually have an amplitude ranging from several centimeters to a few meters and a period of several hours. Therefore, a driving head with an amplitude of 1 m and a period of 12 h was imposed on the sea boundary. The mean sea level was set to 5 m from the aquifer bottom. Since the response time of the unsaturated zone is related to soil properties, two different soils were considered: sand with a weak capillarity and loam with a strong capillarity (Table 2). Again, the MVG model matches well with the VG model for these two soils (Fig. 2). Four different beach slopes were assumed: 30°, 45°, 60° and 90°. Based on the above parameters, ε was calculated to be less than unity even with the static effective porosity, and thus both the previous and present analytical solutions are applicable for all scenarios.

5. Results and discussion

5.1. Vertical flow effects on watertable fluctuations

Compared with previous analytical solutions (Nielsen, 1990; Li et al., 2000a), the new analytical solution involves not only vertical flow, but also the dynamic effective porosity. Therefore, we first examined vertical flow effects on watertable fluctuations based on the new analytical solution by assuming $n_t = n_e$. Fig. 9 displays watertable elevation distributions calculated by different analytical solutions at five typical time slots (i.e., $t = 0$, $T/8$, $T/4$, $3T/8$ and $T/2$) for sand coastal unconfined aquifers with different sea boundary slopes. Note that only the results from the analytical solution of Li et al. (2000a) (without accounting for the vertical flow) are presented for comparison since the predictions from the analytical solution of Nielsen (1990) are similar to those from the analytical solution of Li et al. (2000a). As anticipated, whether considering vertical flow or not, the fluctuation amplitude attenuates as

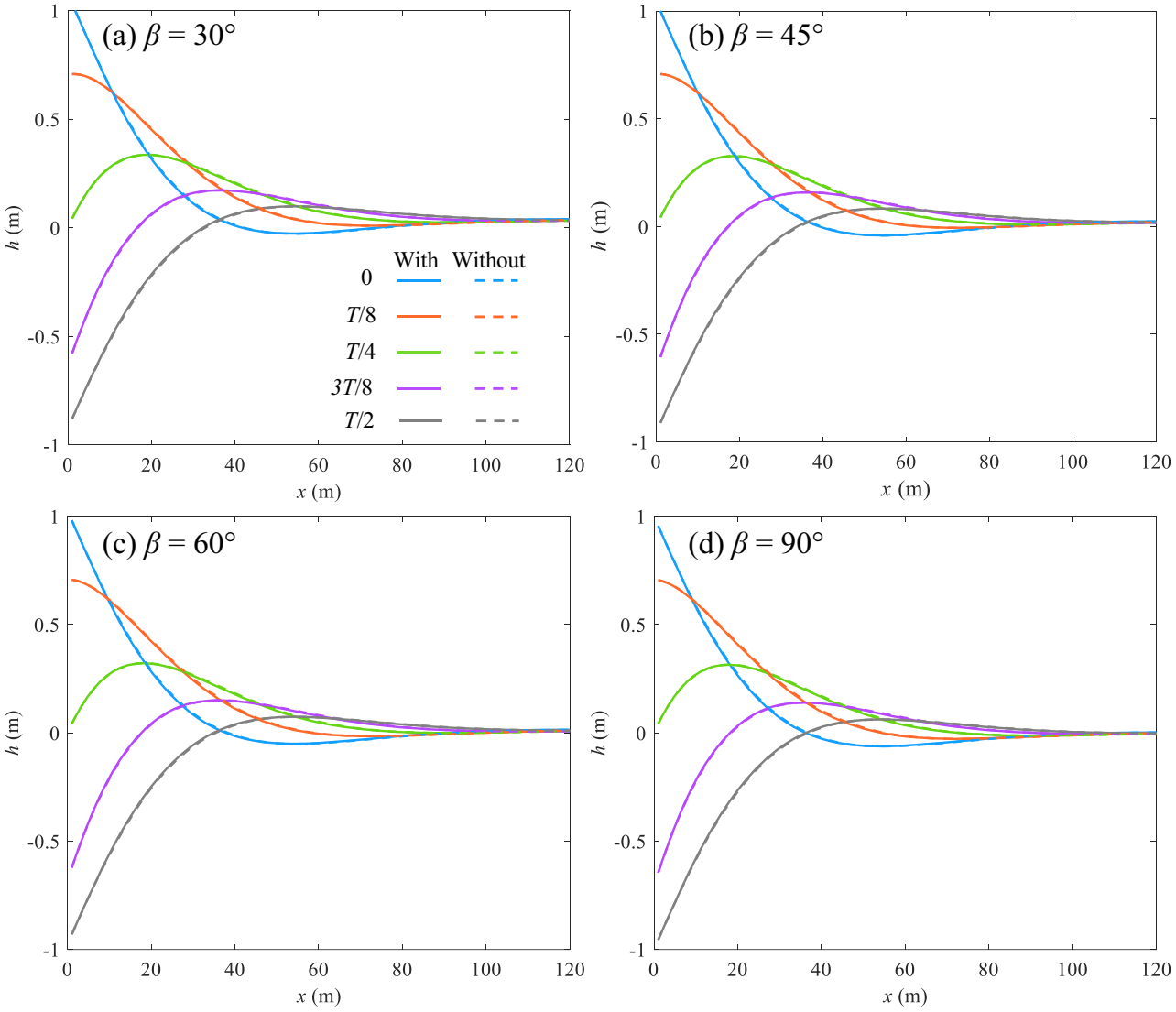

Fig. 12. Predicted watertable elevation distributions of sand coastal unconfined aquifers based on the analytical solutions with (dashed lines) and without (solid lines) considering the dynamic effective porosity at five times: 0 (blue), $T/8$ (orange), $T/4$ (green), $3T/8$ (purple) and $T/2$ (gray). Each plot corresponds to a different sloping sea boundary: (a) 30°, (b) 45°, (c) 60° and (d) 90°.

the watertable waves propagate inland, eventually becoming negligible. At the same time, watertable overheight (the average inland watertable elevation during one period is larger than the mean sea level) occurs (Fig. 9). Note that both analytical solutions predict a zero overheight for $\beta = 90°$ because a linearized governing equation describes watertable fluctuations (Todd and Mays, 2004). By comparison, predictions with the vertical flow are almost identical to the predictions of the Li et al. (2000a) approximation for all beach slopes, suggesting that effects of the vertical flow on watertable elevations are negligible for sand coastal unconfined aquifers.

In contrast to sand aquifers, watertable elevation distributions predicted by the analytical solution with the vertical flow greatly differs from that predicted by the analytical solution without vertical flow for loam coastal unconfined aquifers, regardless of the beach slope (Fig. 10). According to Li et al. (2000b), the effects of the vertical flow depend on the value of $n_e\omega D/K_s$. Specifically, the greater $n_e\omega D/K_s$ is, the more significant are the vertical flow effects. For sand and loam coastal aquifers considered here, $n_e\omega D/K_s$ is 0.1 and 6.19, respectively, confirming the observed increased importance of vertical flow for loam coastal unconfined aquifers. Compared with the predictions of Li et al. (2000a), including the vertical flow leads to a smaller overheight. These results imply that neglecting vertical flow effects may lead to an inappropriate estimate of watertable elevations, especially for aquifers with large $n_e\omega D/K_s$.

To further illustrate vertical flow effects, the predicted watertable elevation time series at $x = 5$ and 50 m for both sand and loam aquifers are presented in Fig. 11. As expected, the watertable wave propagates inland with amplitude decay and phase lag, regardless of whether vertical flow is included. Moreover, both watertable elevation and overheight decrease with increasing the beach slope. This is because increasing the beach slope leads to a decrease of the moving boundary range, which inhibits watertable wave propagation (Li et al., 2000a; Teo et al., 2003). Compared with sand aquifers, the fluctuation amplitude is smaller at a given location for loam aquifers whether predicted by the present analytical solution or that of Li et al. (2000a). However, the predicted overheight is greater for loam aquifers. Again, the difference between the predictions from the previous analytical solution and the present analytical solution can be ignored at both locations for sand coastal unconfined aquifers. Nevertheless, it becomes significant for loam coastal unconfined aquifers. Specifically, the vertical flow has a mild impact on the fluctuation amplitude, while it significantly decreases the phase lag at $x = 5$ m. Consequently, the watertable elevation

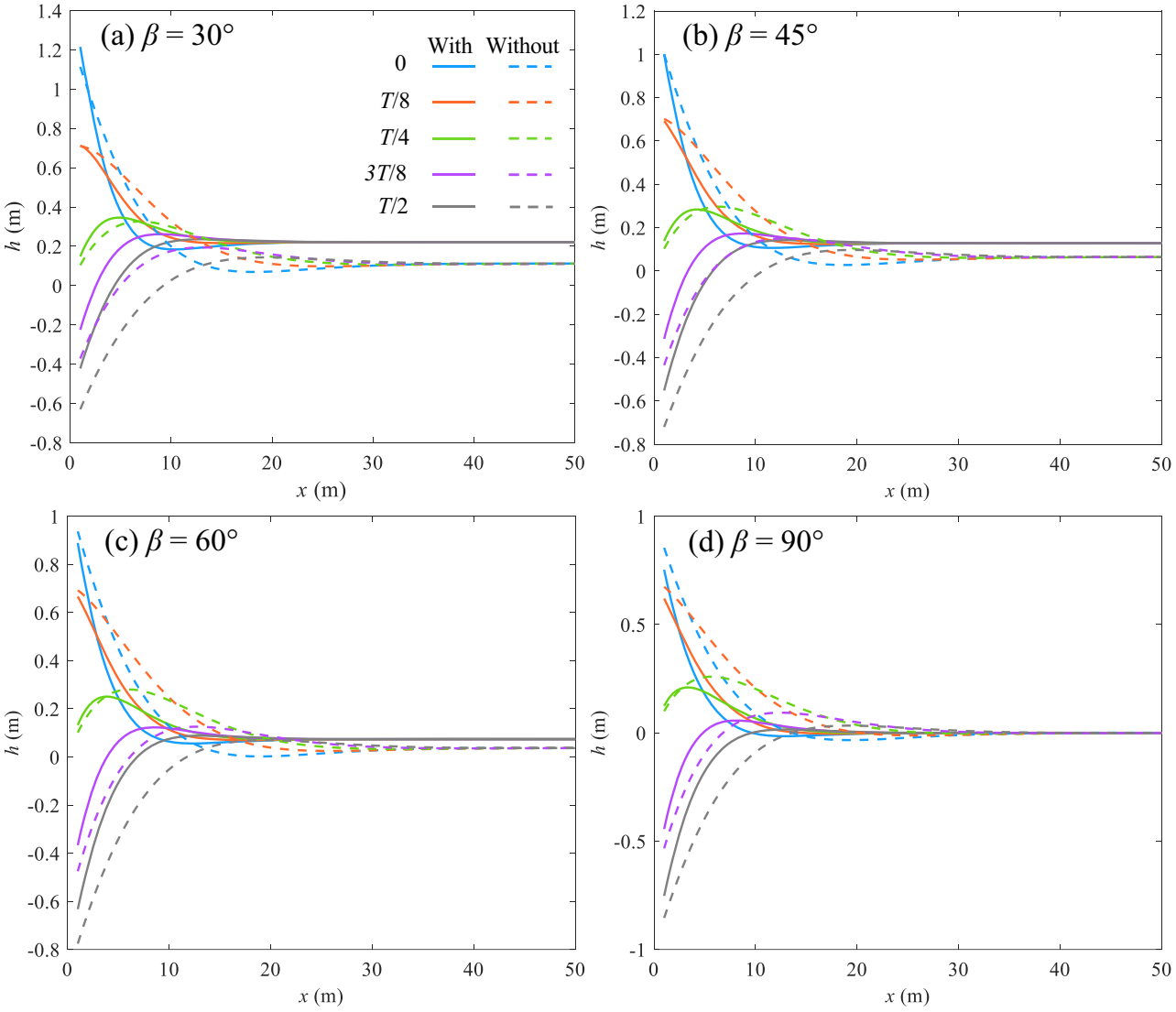

Fig. 13. Predicted watertable elevation distributions of loam coastal unconfined aquifers based on the analytical solutions with (dashed lines) and without (solid lines) considering the dynamic effective porosity at five time: 0 (blue), $T/8$ (orange), $T/4$ (green), $3T/8$ (purple) and $T/2$ (gray). Each plot corresponds to a different sloping sea boundary: (a) 30°, (b) 45°, (c) 60° and (d) 90°.

peaks earlier with vertical flow included. In other words, vertical flow can accelerate watertable wave propagation. As the beach slope increases, the deviation between the predictions with and without accounting for vertical flow decreases. This implies that increasing the beach slope weakens vertical flow effects on watertable fluctuations. Furthermore, for loam coastal unconfined aquifers at $x = 50$ m, the difference between overheights predicted with and without including vertical flow decreases with increasing of the beach slope.

5.2. *Dynamic effective porosity effects on watertable fluctuations*

We investigated dynamic effective porosity effects on watertable fluctuations based on the new analytical solution. Luo et al. (2023) recommended $a = 0.0335$ and $b = 0.4444$ for coastal unconfined aquifers with a vertical sea boundary, and the same values are used here. Fig. 12 compares the watertable elevation distributions for sand coastal unconfined aquifers calculated with the new analytical solution with and without the dynamic effective porosity. Similarly to the case of vertical flow, there is no discernible difference between the predictions with and without the dynamic effective porosity at the five times considered (i.e., $t = 0$, $T/8$, $T/4$, $3T/8$ and $T/2$) for all beach slopes.

However, for loam coastal unconfined aquifers, the predicted watertable elevation distributions with and without consideration of the dynamic effective porosity noticeably deviate (Fig. 13). This emphasizes the critical role played by the dynamic effective porosity in predictions of watertable wave propagation. Compared with the results that ignore the dynamic effective porosity, the fluctuation amplitude is larger at the same location and watertable waves propagate further inland (by a factor of approximately 2) with the dynamic effective porosity included. In addition, including the dynamic effective porosity results in a smaller watertable overheight. As mentioned earlier, a zero overheight for $\beta = 90°$ results from using a linearized governing equation to describe watertable fluctuations.

The effective porosity reflects the vertical water exchange between the saturated and vadose zones. During watertable fluctuations, the dynamic effective porosity is usually less than the static effective porosity since the vadose zone has insufficient time to reach equilibrium. A smaller effective porosity corresponds to reduced vertical water exchange between the saturated and vadose zones, and hence watertable waves can propagate further landward (Li et al., 1997; Luo et al., 2023). For sand coastal unconfined aquifers considered here, $n_e\omega H_\psi/K_s$ is calculated to be 0.002, which gives a dynamic effective porosity of

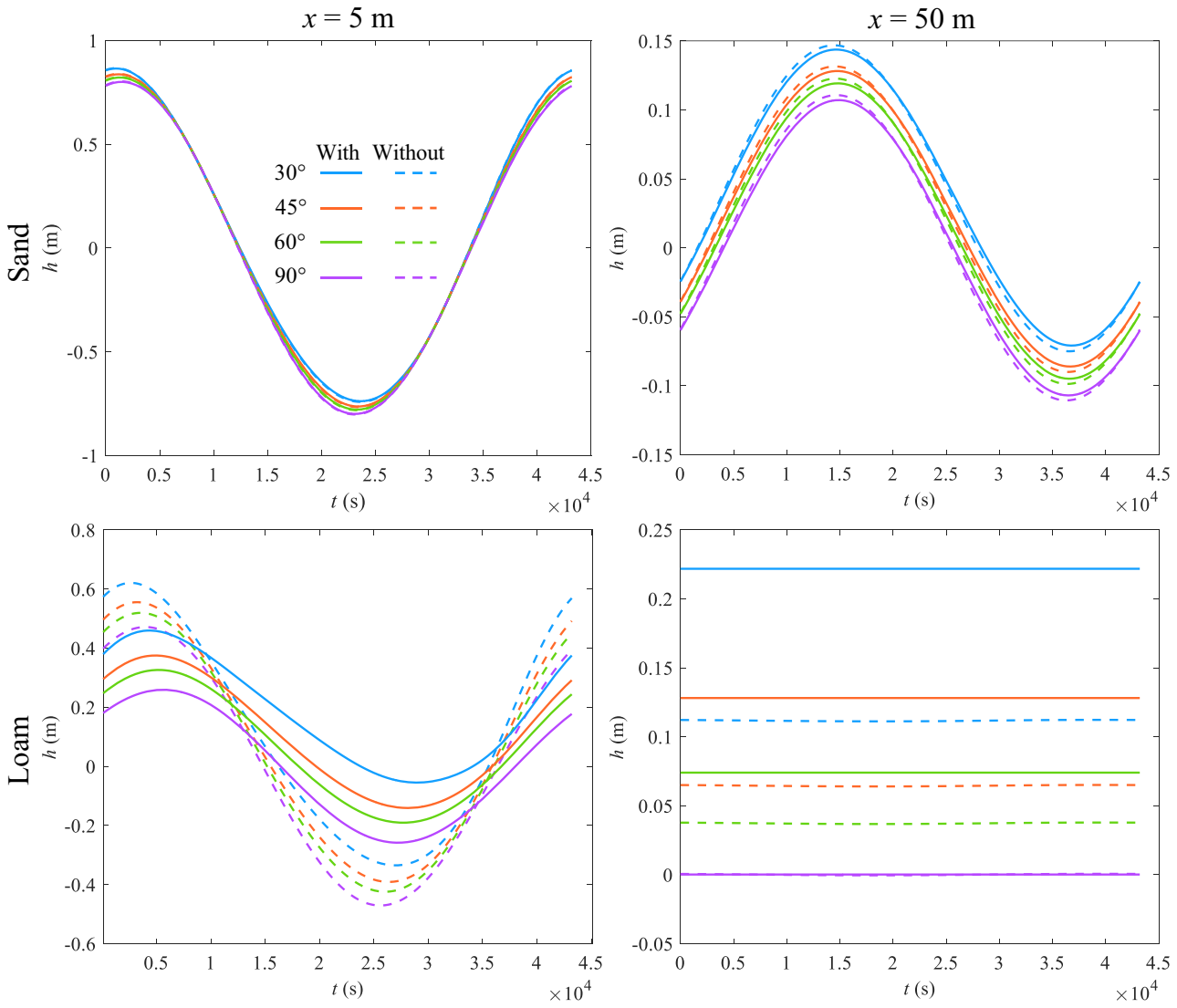

Fig. 14. Watertable elevation time series calculated from the analytical solutions with (dashed lines) and without (solid lines) considering the dynamic effective porosity at $x = 5$ m (left panel) and 50 m (right panel) for sand (top panel) and loam (bottom panel) coastal unconfined aquifers with a different sloping sea boundary: 30° (blue), 45° (orange), 60° (green) and 90° (purple).

0.39, almost equal to the static effective porosity (0.4). However, for loam coastal aquifers, $n_e\omega H_\psi/K_s$ is 0.82 and the dynamic effective porosity (0.059) is much less than the static porosity (0.23). This means that, due to capillarity, the vadose zone has insufficient time to respond to watertable fluctuations for loam coastal unconfined aquifers. Therefore, the dynamic effective porosity plays a more important role in affecting watertable fluctuations for loam coastal unconfined aquifers. This result is consistent with the finding of Luo et al. (2023) who indicated that the effects of the dynamic effective porosity depend on the value of $n_e\omega H_\psi/K_s$. The greater $n_e\omega H_\psi/K_s$ is, the more significant dynamic effective porosity effects are.

Similarly, to further examine the effects of the dynamic effective porosity on watertable fluctuations, watertable elevation time series at $x = 5$ and 50 m are plotted for both sand and loam coastal unconfined aquifers (Fig. 14). As can be seen, the difference between the predictions from the analytical solutions with and without considering the dynamic effective porosity can be ignored for both locations of sand coastal unconfined aquifers, while it is pronounced for loam coastal unconfined aquifers. At $x = 5$ m, the dynamic effective porosity not only decreases the phase lag, but also significantly amplifies the fluctuation amplitude for loam coastal unconfined aquifers, regardless of the beach slope. Consequently, watertable fluctuations can propagate further inland if the dynamic effective porosity is accounted for. This differs from the role played by the vertical flow, which mainly alters the phase lag. In general, the deviation between the predictions with and without consideration of the dynamic effective porosity decreases with increasing beach slope, implying that a steep beach slope weakens dynamic effective porosity effects on watertable fluctuations. Additionally, at $x = 50$ m for the loam coastal unconfined aquifer, the difference between overheights calculated with and without the dynamic effective porosity decreased with increasing beach slope.

6. Conclusions

This study evaluated the effects of the vertical flow and dynamic effective porosity on watertable fluctuations in coastal unconfined aquifers with a sloping sea boundary. Using a perturbation method, we derived an analytical solution to the modified Boussinesq equation developed by Luo et al. (2023) for coastal unconfined aquifers with a sloping sea boundary. After comparing with a well-validated numerical model, this analytical solution was used to explore the effects of the vertical flow and dynamic effective porosity on watertable fluctuations.

The following conclusions can be reached:

(1) The new analytical solution accurately predicts watertable fluctuations in coastal unconfined aquifers with a sloping sea boundary, highlighting the importance of vertical flow and dynamic effective porosity effects.
(2) Vertical flow has a minor influence on the watertable fluctuation amplitude while it significantly decreases the phase lag at a given location, regardless of the beach slope. Compared with sand coastal unconfined aquifers, vertical flow effects on watertable fluctuations are more significant for loam coastal unconfined aquifers.
(3) In contrast to the vertical flow, considering the dynamic effective porosity not only accentuates the fluctuation amplitude, but also decreases the phase lag at a given location. Compared with sand aquifers, due to capillarity the dynamic effective porosity plays a more important role in affecting watertable fluctuations for loam coastal unconfined aquifers.
(4) Increasing the beach slope weakens the effects of the vertical flow and dynamic effective porosity on watertable fluctuations.
(5) Including either the vertical flow or dynamic effective porosity leads to a lower phase-averaged watertable overheight. Moreover, the difference between overheights for sand and loam aquifers calculated with and without the vertical flow/dynamic effective porosity decreases with increasing the beach slope.

In reality, coastal unconfined aquifers are expected to have complex geometries that lead to three-dimensional groundwater flow. In addition, the sea boundary is subject to waves rather than a regular signal considered here, which makes watertable fluctuations more complicated (Nielsen, 2009). Despite this, the new analytical solution can be used as a simple tool to predict watertable fluctuations that are fundamental for understanding many groundwater-dependent processes in coastal unconfined aquifers with sloping sea boundaries.

Data availability

The experimental data used in this study are compiled from Cartwright et al. (2004). The analytical solution code can be found at https://doi.org/10.5281/zenodo.8019310.

CRediT authorship contribution statement

Zhaoyang Luo: Conceptualization, Methodology, Visualization, Writing – original draft, Writing – review & editing. **Jun Kong:** Methodology, Supervision, Writing – review & editing. **D.A. Barry:** Methodology, Supervision, Writing – review & editing.

Declaration of Competing Interest

The authors declare that they have no known competing financial interests or personal relationships that could have appeared to influence the work reported in this paper.

Acknowledgments

JK acknowledges the National Natural Science Foundation of China (51979095). The authors thank Xiayang Yu for generating the log-normal hydraulic conductivity field.

References

Bakhtyar, R., Brovelli, A., Barry, D.A., Li, L., 2011. Wave-induced water table fluctuations, sediment transport and beach profile change: Modeling and comparison with large-scale laboratory experiments. Coastal Eng. 58 (1), 103–118. https://doi.org/10.1016/j.coastaleng.2010.08.004.

Barry, D.A., Barry, S.J., Parlange, J.-Y., 1996. Capillarity correction to periodic solutions of the shallow flow approximation, In: C.B. Pattiaratchi (Ed.), *Mixing Processes in Estuaries and Coastal Seas, Coastal and Estuarine Studies*, Volume 50, American Geophysical Union, Washington, DC, pp. 496-510. https://doi.org/10.1029/CE050.

Bear, J., 2012. *Hydraulics of Groundwater*. Dover Publications, Inc., Mineola, New York.

Cartwright, N., Nielsen, P., Dunn, S., 2003. Water table waves in an unconfined aquifer: Experiments and modeling. Water Resour. Res. 39 (12), 1330. https://doi.org/10.1029/2003WR002185.

Cartwright, N., Nielsen, P., Li, L., 2004. Experimental observations of watertable waves in an unconfined aquifer with a sloping boundary. Adv. Water Resour. 27 (10), 991–1004. https://doi.org/10.1016/j.advwatres.2004.08.006.

Cartwright, N., Nielsen, P., Perrochet, P., 2005. Influence of capillarity on a simple harmonic oscillating water table: Sand column experiments and modeling. Water Resour. Res. 41 (8), W08416. https://doi.org/10.1029/2005WR004023.

Childs, E.C., 1960. The nonsteady state of the water table in drained land. J. Geophys. Res. 65 (2), 780–782. https://doi.org/10.1029/JZ065i002p00780.

Heiss, J.W., Michael, H.A., 2014. Saltwater-freshwater mixing dynamics in a sandy beach aquifer over tidal, spring-neap, and seasonal cycles. Water Resour. Res. 50 (8), 6747–6766. https://doi.org/10.1002/2014WR015574.

Jeng, D.S., Mao, X., Enot, P., Barry, D.A., Li, L., 2005a. Spring-neap tide-induced beach water table fluctuations in a sloping coastal aquifer. Water Resour. Res. 41 (7), W07026. https://doi.org/10.1029/2005WR003945.

Jeng, D.S., Seymour, B.R., Barry, D.A., Li, L., Parlange, J.-Y., 2005b. New approximation for free surface flow of groundwater: Capillarity correction. Adv. Water Resour. 28 (10), 1032–1039. https://doi.org/10.1016/j.advwatres.2004.05.012.

Kong, J., Song, Z., Xin, P., Shen, C., 2011. A new analytical solution for tide-induced groundwater fluctuations in an unconfined aquifer with a sloping beach. China Ocean Eng. 25 (3), 479–494. https://doi.org/10.1007/s13344-011-0039-0.

Kong, J., Shen, C.J., Xin, P., Song, Z., Li, L., Barry, D.A., Jeng, D.S., Stagnitti, F., Lockington, D.A., Parlange, J.-Y., 2013. Capillary effect on water table fluctuations in unconfined aquifers. Water Resour. Res. 49 (5), 3064–3069. https://doi.org/10.1002/wrcr.20237.

Kong, J., Xin, P., Hua, G.F., Luo, Z.Y., Shen, C.J., Chen, D., Li, L., 2015. Effects of vadose zone on groundwater table fluctuations in unconfined aquifers. J. Hydrol. 528, 397–407. https://doi.org/10.1016/j.jhydrol.2015.06.045.

Kong, J., Luo, Z., Shen, C., Hua, G., Zhao, H., 2016a. An alternative Boussinesq equation considering the effect of hysteresis on coastal groundwater waves. Hydrol. Process. 30 (15), 2657–2670. https://doi.org/10.1002/hyp.10810.

Kong, J., Shen, C., Luo, Z., Hua, G., Zhao, H., 2016b. Improvement of the hillslope-storage Boussinesq model by considering lateral flow in the unsaturated zone. Water Resour. Res. 52 (4), 2965–2984. https://doi.org/10.1002/2015WR018054.

Li, L., Barry, D.A., Parlange, J.-Y., Pattiaratchi, C.B., 1997. Beach water table fluctuations due to wave run-up: Capillarity effects. Water Resour. Res. 33 (5), 935–945. https://doi.org/10.1029/96WR03946.

Li, L., Barry, D.A., Stagnitti, F., Parlange, J.-Y., 1999. Submarine groundwater discharge and associated chemical input to a coastal sea. Water Resour. Res. 35 (11), 3253–3259. https://doi.org/10.1029/1999WR900189.

Li, L., Barry, D.A., Stagnitti, F., 2000a. Beach water table fluctuations due to spring-neap tides: Moving boundary effects. Adv. Water Resour. 23 (8), 817–824. https://doi.org/10.1016/S0309-1708(00)00017-8.

Li, L., Barry, D.A., Stagnitti, F., Parlange, J.-Y., 2000b. Groundwater waves in a coastal aquifer: A new governing equation including vertical effects and capillarity. Water Resour. Res. 36 (2), 411–420. https://doi.org/10.1029/1999WR900307.

Luo, Z., Kong, J., Shen, C., Lu, C., Hua, G., Zhao, Z., Zhao, H., Li, L., 2019. Evaluation and application of the modified van Genuchten function for unsaturated porous media. J. Hydrol. 571, 279–287. https://doi.org/10.1016/j.jhydrol.2019.01.051.

Luo, Z., Kong, J., Yao, L., Lu, C., Li, L., Barry, D.A., 2023. Dynamic effective porosity explains laboratory experiments on watertable fluctuations in coastal unconfined aquifers. Adv. Water Resour. 171, 104354 https://doi.org/10.1016/j.advwatres.2022.104354.

Moore, W.S., 2010. The effect of submarine groundwater discharge on the ocean. Annu. Rev. Mar. Sci. 2 (1), 59–88. https://doi.org/10.1146/annurev-marine-120308-081019.

Nielsen, P., Aseervatham, R., Fenton, J.D., Perrochet, P., 1997. Groundwater waves in aquifers of intermediate depths. Adv. Water Resour. 20 (1), 37–43. https://doi.org/10.1016/S0309-1708(96)00015-2.

Nielsen, P., 1990. Tidal dynamics of the water table in beaches. Water Resour. Res. 26 (9), 2127–2134. https://doi.org/10.1029/WR026i009p02127.

Nielsen, P., 2009. Coastal and estuarine processes. In: *Advanced Series on Ocean Engineering*, 29. World Scientific Publishing Company, Singapore. https://doi.org/10.1142/7114.

Parlange, J.-Y., Brutsaert, W., 1987. A capillarity correction for free surface flow of groundwater. Water Resour. Res. 23 (5), 805–808. https://doi.org/10.1029/WR023i005p00805.

Parlange, J.-Y., Stagnitti, F., Starr, J.L., Braddock, R.D., 1984. Free-surface flow in porous media and periodic solution of the shallow-flow approximation. J. Hydrol. 70 (1–4), 251–263. https://doi.org/10.1016/0022-1694(84)90125-2.

Pozdniakov, S.P., Wang, P., Lekhov, V.A., 2019. An approximate model for predicting the specific yield under periodic water table oscillations. Water Resour. Res. 55 (7), 6185–6197. https://doi.org/10.1029/2019WR025053.

Rabinovich, A., Barrash, W., Cardiff, M., Hochstetler, D.L., Bakhos, T., Dagan, G., Kitanidis, P.K., 2015. Frequency dependent hydraulic properties estimated from oscillatory pumping tests in an unconfined aquifer. J. Hydrol. 531, 2–16. https://doi.org/10.1016/j.jhydrol.2015.08.021.

Raubenheimer, B., Guza, R.T., Elgar, S., 1999. Tidal water table fluctuations in a sandy ocean beach. Water Resour. Res. 35 (8), 2313–2320. https://doi.org/10.1029/1999WR900105.

Robinson, C., Gibbes, B., Li, L., 2006. Driving mechanisms for groundwater flow and salt transport in a subterranean estuary. Geophys. Res. Lett. 33 (3), L03402. https://doi.org/10.1029/2005GL025247.

Robinson, C.E., Xin, P., Santos, I.R., Charette, M.A., Li, L., Barry, D.A., 2018. Groundwater dynamics in subterranean estuaries of coastal unconfined aquifers: Controls on submarine groundwater discharge and chemical inputs to the ocean. Adv. Water Resour. 115, 315–331. https://doi.org/10.1016/j.advwatres.2017.10.041.

Shoushtari, S.M.H.J., Cartwright, N., Nielsen, P., Perrochet, P., 2016. The effects of oscillation period on groundwater wave dispersion in a sandy unconfined aquifer: Sand flume experiments and modelling. J. Hydrol. 533, 412–420. https://doi.org/10.1016/j.jhydrol.2015.12.032.

Teo, H.T., Jeng, D.S., Seymour, B.R., Barry, D.A., Li, L., 2003. A new analytical solution for water table fluctuations in coastal aquifers with sloping beaches. Adv. Water Resour. 26 (12), 1239–1247. https://doi.org/10.1016/j.advwatres.2003.08.004.

Todd, D.K., Mays, L.W., 2004. Groundwater Hydrology, 3rd Edition. John Wiley & Sons, Hoboken, New Jersey.

Troch, P. (1993). *Conceptual basin-scale runoff process models for humid catchments: analysis, synthesis and applications*. RUG. Faculteit Landbouwkundige en Toegepaste Biologische Wetenschappen. http://hdl.handle.net/1854/LU-8566676, last accessed 11 June 2023.

van Genuchten, M.T., 1980. A closed-form equation for predicting the hydraulic conductivity of unsaturated soils. Soil Sci. Soc. Am. J. 44 (5), 892–898. https://doi.org/10.2136/sssaj1980.03615995004400050002x.

Vos, K., Harley, M.D., Splinter, K.D., Walker, A., Turner, I.L., 2020. Beach slopes from satellite-derived shorelines. Geophys. Res. Lett. 47 (14), e2020GL088365 https://doi.org/10.1029/2020GL088365.

Voss, C.I., & Provost, A.M. (2008). *SUTRA: A model for saturated-unsaturated, variable density groundwater flow with solute or energy transport (Rep.02–4231)*. Reston, VA: U. S. Geological Survey. https://water.usgs.gov/nrp/gwsoftware/sutra/SUTRA_2_2-documentation.pdf, last accessed 11 June 2023.

Werner, A.D., Bakker, M., Post, V.E.A., Vandenbohede, A., Lu, C., Ataie-Ashtiani, B., Simmons, C.T., Barry, D.A., 2013. Seawater intrusion processes, investigation and management: Recent advances and future challenges. Adv. Water Resour. 51, 3–26. https://doi.org/10.1016/j.advwatres.2012.03.004.

Xin, P., Robinson, C., Li, L., Barry, D.A., Bakhtyar, R., 2010. Effects of wave forcing on a subterranean estuary. Water Resour. Res. 46 (12), W12505. https://doi.org/10.1029/2010WR009632.

Yu, X., Xin, P., Luo, Z., Pu, L., 2023. Thermal effects of freshwater injection on flow and salinity distributions in tidally-affected coastal unconfined aquifers. J. Hydrol. 622, 129739 https://doi.org/10.1016/j.jhydrol.2023.129739.

Zheng, Y., Yang, M., Liu, H., 2022. The effects of truncating the capillary fringe on water–table dynamics during periodic forcing. Water Resour. Res. 58 (1), e2021WR031112 https://doi.org/10.1029/2021WR031112.